Modularized, Reconfigurable and Bidirectional Charging Infrastructure for Electric Vehicles with Silicon Carbide Power Electronics (MoReSiC)

Deliverable D3.2 (Month 19)

Title: "Electrical and thermal models of the multiport isolated DC/DC converter"

Authors: Dimosthenis Peftitsis, Kaushik Naresh Kumar
Norwegian University of Science and Technology

February 2023

Executive summary

This deliverable D3.2 presents the electrical and thermal models of the modular and multiport DC/DC power electronic converters, which are suitable for designing and operating modularized, reconfigurable, and bidirectional chargers for electric vehicles. The fundamental circuits and the topology configuration of each multiport DC/DC converter are presented and analysed. Four topologies are considered here; two of them utilize the two-level full-bridge as the fundamental circuit and two are hybrid designs utilizing two-level full-bridge and active neutral-point clamp circuits. The detailed electrical and thermal models of these four converters designed with Silicon Carbide metal oxide semiconductor field-effect transistors are presented. Moreover, the converters' performance in terms of power losses, efficiency, temperature distribution among the circuits and power semiconductor requirements is shown. The results presented in this document have been acquired through theoretical analysis, as well as electrical and thermal simulations.

Table of Contents

1. Modular and Multiport DC/DC converter configurations

Based on a thorough theoretical and simulation study, **four reconfigurable** isolated DC/DC power converter configurations have been identified as potential candidates for modularized and reconfigurable charging stations for electric vehicles (EVs). In order to ensure reconfigurability and modularity, the main idea is to design these converters using a standardized and fundamental building block, namely module. After the overall assessment, two fundamental building blocks have been chosen: the full-bridge (FB) circuit and the active neutral-point clamped (ANPC) circuit, as shown in Figs. 1 (e) and (f), respectively.

To increase the flexibility in terms of voltage and electric power supply or under input supply conditions imposing higher voltages, FB and ANPC circuits can be connected in series or in parallel to meet the design constraints. The two most suitable modular isolated DC/DC converters for the application under study are shown in Figs. 1 (a) and (b). The first configuration is based on a classical FB-FB Dual Active Bridge (DAB) converter comprising input series FB modules, while the FB modules on the output stage can either be connected in parallel for increasing current capability or in series for higher supplied voltage. A possible way to enable reconfigurability on the output stage is the use of mechanical relays or solid-state breakers (e.g., S1, S2 and S3 in Fig. 1(a)). The second isolated DC/DC converter configuration is designed by series connection of two ANPC modules on the input stage and the use of FB modules on the output as shown in Fig. 1(b). Reconfigurability of the output stage (i.e., parallel or series connection) in this ANPC-FB DAB is also achieved by means of mechanical relays or solid-state breakers. It should be noted that for the configuration of Figs. 1(a) and (b), the required transformer (T/F) is designed with a single primary and a single secondary winding.

The fundamental circuits can also be combined to design multi-port (MP) converter configurations as shown in Figs. 1 (c) and (d). Both figures show three-port isolated DC/DC converters, which utilize a single multi-winding high-frequency T/F, which has a smaller volume and weight than the modular configurations with multiple transformers. Fig. 1(c) illustrates a three-port converter comprising a FB module on the input stage which feeds the primary winding of the multi-winding T/F. On the output stage of this configuration there are two FB modules, each supplied by a separate secondary winding of the T/F. As in the case of the modular converters, the output stage of the three-port converter of Fig. 1(c) can either be connected in series or in parallel, depending on the load requirements. The second MP configuration contains an ANPC module on the input stage that feeds the primary winding of the multi-winding T/F. On the output stage, there are two FB modules, which are supplied separately by each of the two secondary T/F's windings. The two FB modules on the output have the flexibility of either series or parallel connection.

Each of the four evaluated topologies can be configured to one of three configuration option shown at the bottom of Fig. 1. According to each option, the reconfigurable converter can supply:

(i) Option 1: one 800V battery at rated power or
(ii) Option 2: one 400V battery at rated power or
(iii) Option 3: two 400V batteries each at half of the rated power.

This is achieved by controlling the switches S1, S2 and S3 dynamically.

Given the bipolar DC bus at the charging station (Fig. 2), various ways of connecting the four reconfigurable isolated DC/DC converters emerge. In particular, the input stage of the converters can either be connected between the positive and midpoint (i.e., Vdc+ and 0), midpoint and negative (i.e., 0 and Vdc-) or between positive and negative (i.e., Vdc+ and Vdc-) with the 0 acting as the midpoint. As it will be shown later in this report, the ANPC module of the three-port ANPC-FB configuration can be connected to any of these three ways. However, it should be noted that connecting the ANPC module between Vdc+ and Vdc-, imposes the need for power devices having larger voltage ratings compared to ANPC modules suitable for connection between Vdc+ and 0 or 0 and Vdc-.

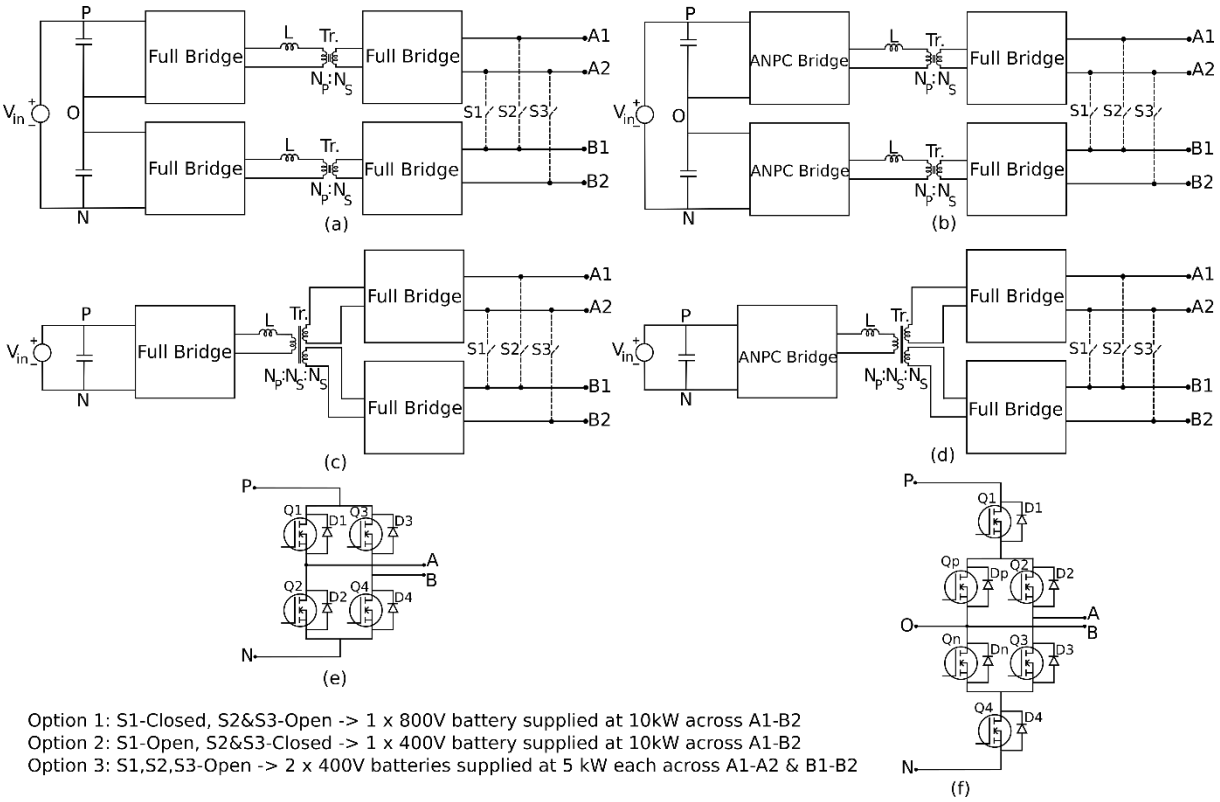

Fig. 1: Block diagrams of the evaluated topologies: (a) FB-FB modular DAB, (b) ANPC-FB modular DAB, (c) Three-port FB-FB DAB, (d) Three-port ANPC-FB DAB, (e) Full bridge, and (f) ANPC bridge.

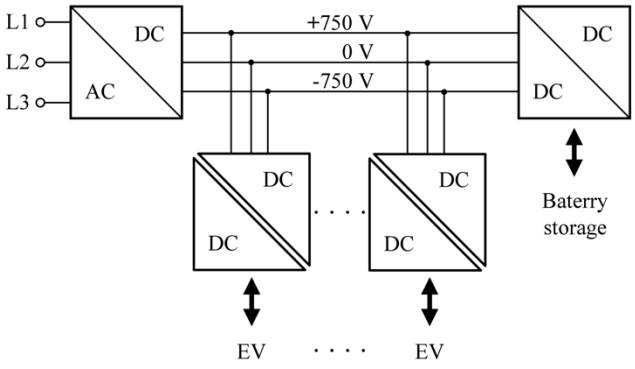

Fig. 2: Schematic of the EV Charging system based on bipolar DC bus.

The DC bus of the charging station operates at a nominal voltage of 1.5 kV, which -considering the bipolar DC bus- is divided to a voltage of Vdc+=750 V and Vdc-=-750 V referred to the

midpoint 0. These nominal voltage values dictate the voltage class of the SiC MOSFETs employed in the reconfigurable DC/DC converters. All the considered topologies are evaluated for a total power transfer of 10 kW, supplying an output voltage of 800V across the battery load (i.e., Option 1: series connection of the secondary bridges).

The first modular isolated DC/DC converter configuration (FB-FB modular DAB, Fig. 1(a)) consists of two series-connected FB circuits. Each of the FB modules should be able to sustain a blocking voltage of 750 V and, thus, these employ 1.2-kV class power devices.

The second modular configuration (Fig. 1(b)) is based on two series connected ANPC modules on the input stage. Each of these modules is supplied with 750 V; however, only half of this voltage must be blocked by the power devices. Thus, it is sufficient that the SiC MOSFETs on the ANPC module are rated at 650 V.

The three-port FB-FB DAB (Fig. 1(c)) employs a single FB module on the input stage. Two options for connectivity and choice of power devices emerge. If the FB module is connected between Vdc+ and 0 or between 0 and Vdc-, it should only block 750V and therefore, 1.2-kV class Silicon Carbide (SiC) metal oxide semiconductor field-effect transistors (MOSFETs) are sufficient. However, in case the FB module is connected across Vdc+ and Vdc-, then the SiC MOSFETs must block 1.5 kV, that impose the need for 3.3-kV class SiC MOSFETs. The latter case is left out of investigation for this deliverable.

A larger degree of flexibility in terms of power devices selection for the modules on the input stage, occurs for the three-port ANPC-FB DAB configuration, shown in Fig. 1(d). The ANPC module can either be connected between Vdc+ and 0, or 0 and Vdc-, or in the bipolar bus of Vdc+ and Vdc-. In case the ANPC should sustain 750 V, the employed power devices should be rated at 650 V and thus will be able to safely block half of the input voltage (750/2=375 V). On the other hand, if the input ANPC module is connected across Vdc+ and Vdc-, the SiC MOSFETs must safely block 750 V, and hence 1.2-kV class devices are required.

For all four configurations, the FB modules on the output supply 400 V and therefore, 650-V class SiC MOSFETs are suitable devices.

2. Electrical and thermal models

For the electrical and thermal modelling of the reconfigurable converters presented in Section 1, two simulation tools, namely LTSPICE and PLECS, were used. LTSPICE is a software tool for semiconductor-device-level modelling and simulations. In this project, LTSPICE was used for modelling and simulating the switching performance of SiC MOSFETs. PLECS is suitable for system-level electrical and thermal modelling and simulations of power converters. PLECS was used for electrical modelling (i.e., circuit and modulation) and thermal modelling (i.e., power losses and temperature) of the reconfigurable DC/DC power converters. More specifically, to enable thermal modelling and simulations of power semiconductor devices in PLECS, SiC MOSFETs are still modelled as ideal switches, but their switching energies are included in the models as look-up tables. A way to obtain the loss data for such models is to use the models from the manufacturers directly. Another possibility is to update these look-up tables using experimental loss data or simulation data by running LTSPICE simulations.

Table I contains the information about the SiC MOSFETs types and ratings used in simulations. The selection of SiC MOSFETs was made considering the type of the fundamental bridge circuit (i.e., FB or ANPC), considered voltage and power levels, better switching performance in terms of faster switching transients due to lower stray inductance in the gate loop (four-pin devices with Kelvin-Source connection) and their availability in the market.

Table I: MOSFET model information and parameters

Topology	MOSFET used in primary bridge	MOSFET used in secondary bridge
FB-FB modular DAB	NTH4L040N120SC1[1]	C3M0015065K[2]
ANPC-FB modular DAB	IMZA65R039M1HXKSA1[3]	C3M0015065K[2]
Three-port FB-FB DAB	NTH4L040N120SC1[1]	C3M0015065K[2]
Three-port ANPC-FB DAB (V_{in} = 750V)	IMZA65R039M1HXKSA1[3]	C3M0015065K[2]
Three-port ANPC-FB DAB (V_{in} = 1500V)	NTH4L040N120SC1[1]	C3M0015065K[2]

[1]1200V, 40mΩ, 58A SiC MOSFET from ON Semiconductor
[2]650V, 15mΩ,120A SiC MOSFET from CREE
[3]650V, 39mΩ, 50A SiC MOSFET from Infineon

The PLECS simulation model for C3M0015065K SiC MOSFET was provided on the manufacturer's (i.e., Wolfspeed) webpage. The PLECS models for the NTH4L040N120SC1 (from ON semiconductor) and IMZA65R039M1HXKSA1 (from Infineon) were developed using parameters extracted from their respective datasheets and by conducting simulations using their LTSPICE models.

The LTSPICE models were used for the estimation of turn-on and turn-off switching energies while the conduction loss data was obtained from the datasheets. Fig. 3 shows the double-pulse circuit LTSPICE simulation model for estimating the switching energies for the IMZA65R039M1HXKSA1 SiC MOSFET at a drain-source voltage of 400V and varied values of drain currents and junction temperatures. Similarly, the LTSPICE model of the double-pulse test circuit for the NTH4L040N120SC1 SiC MOSFET at a blocking voltage of 800 Vis shown in Fig. 4. The libraries for both SiC MOSFET devices were provided by the manufacturers. These models are easily reconfigurable in terms of investigated voltage and current values.

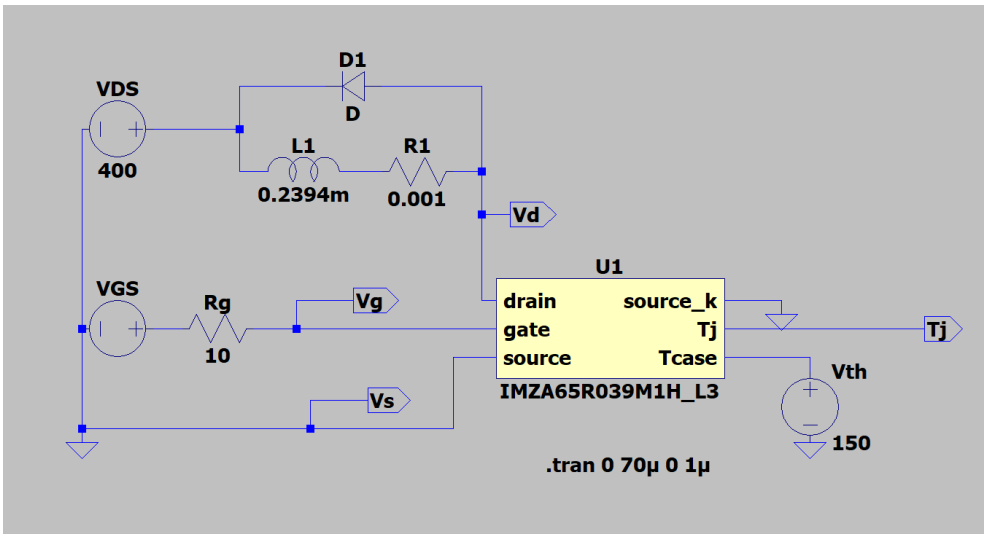

Fig. 3: LTSPICE simulation circuit to estimate switching energy of IMZA65R039M1HXKSA1 SiC MOSFET.

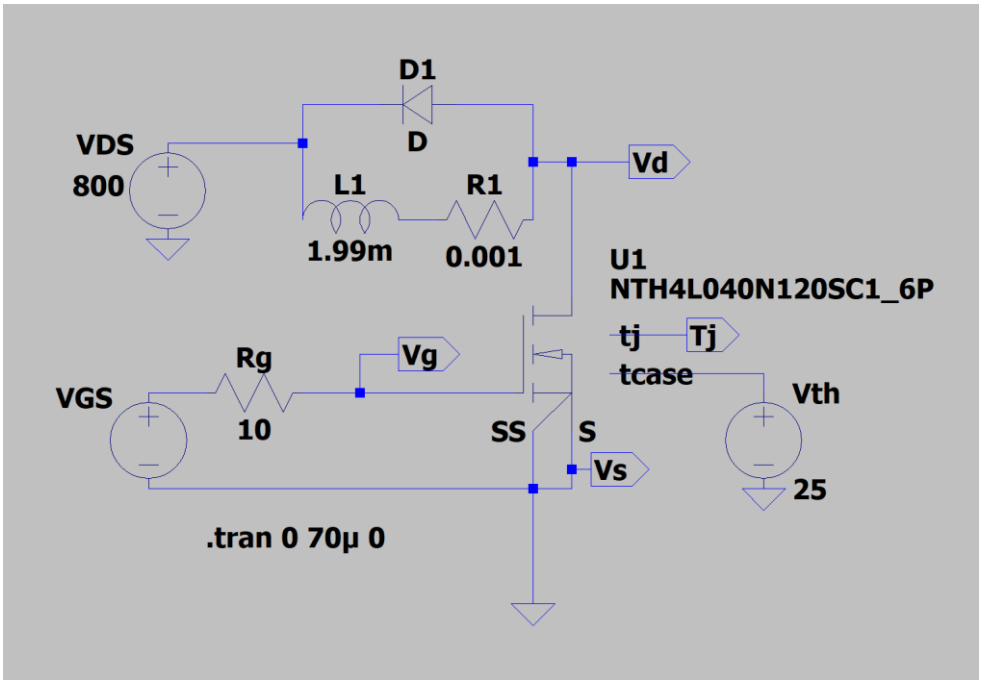

Fig. 4: LTSPICE simulation circuit to estimate switching energy of NTH4L040N120SC1 SiC MOSFET.

The simulated turn-on process of the IMZA65R039M1HXKSA1 SiC MOSFET including the turn-on energy curve at Vds=400V, Id=50A and a junction temperature of T = 150^{o}C is shown in Fig. 5. Fig. 6 illustrates the same simulated parameters for the NTH4L040N120SC1 device at Vds=800V, Id=12A and T = 25^{o}C. The simulated turn-off process and turn-off energy curves for these two SiC MOSFET devices are plotted in Figs. 7 and 8.

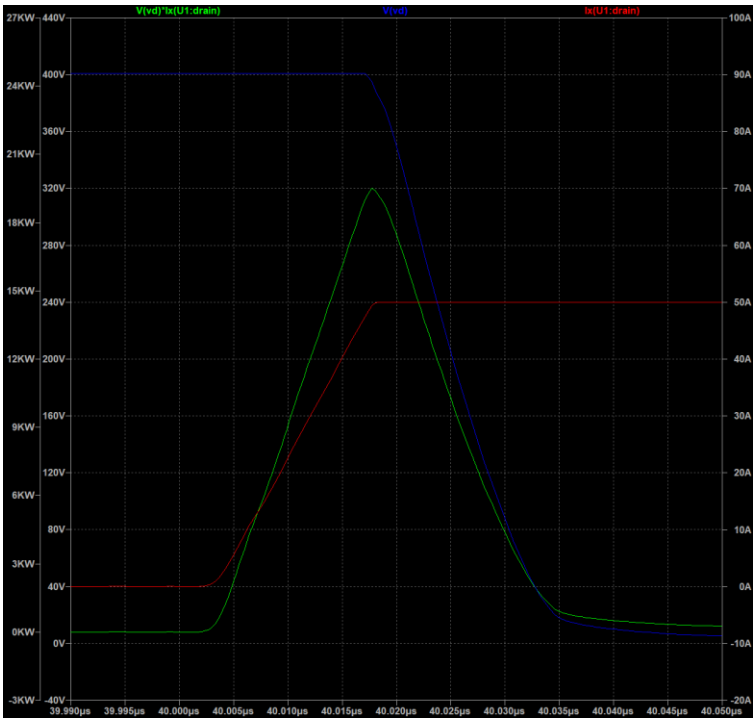

Fig. 5: Simulated turn-on transient and turn-on loss estimation for IMZA65R039M1HXKSA1 at Vds=400V, Id=50A and T = 150ºC.

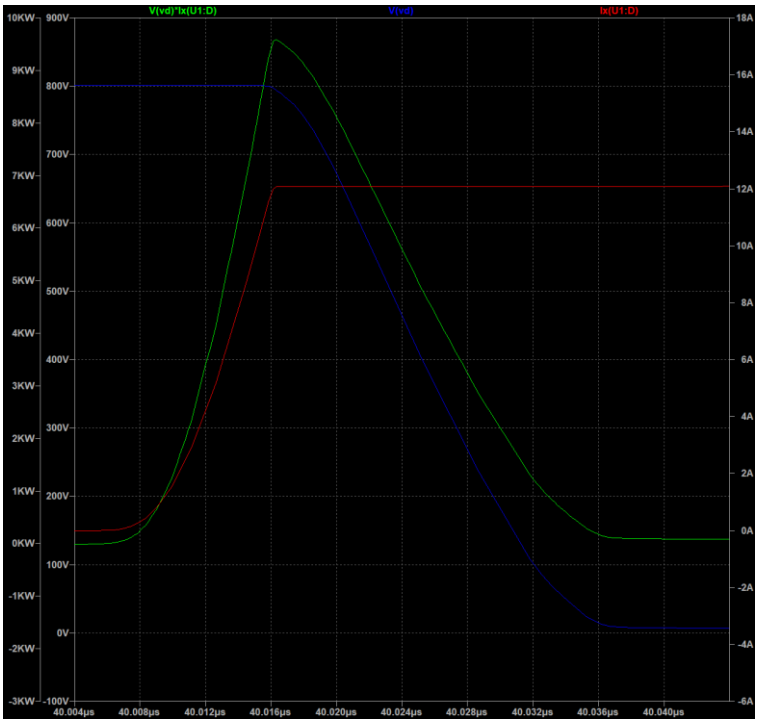

Fig. 6: Simulated turn-on transient and turn-on loss estimation for NTH4L040N120SC1 at Vds=800V, Id=12A and T = 25ºC.

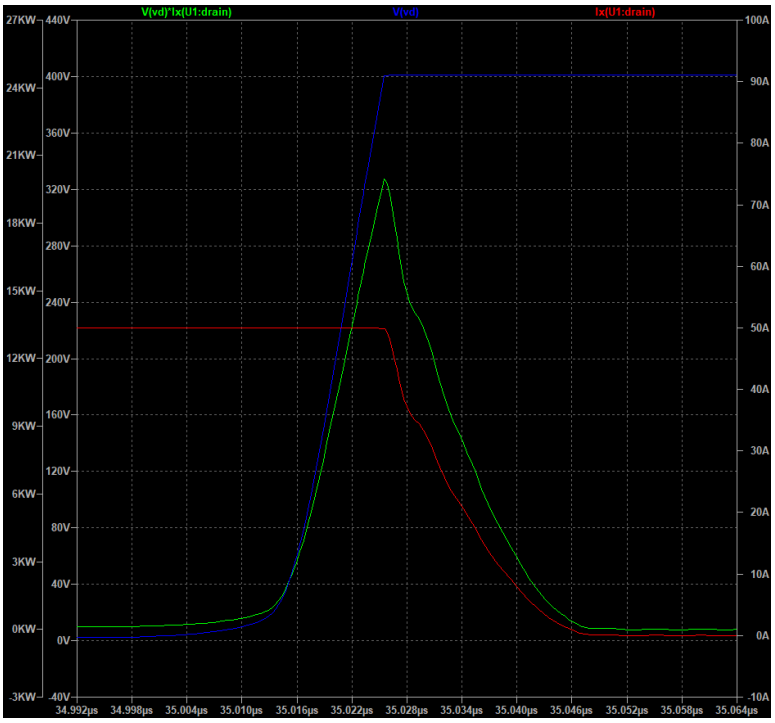

Fig. 7: Simulated turn-off transient and turn-off loss estimation for IMZA65R039M1HXKSA1 at Vds=400V, Id=50A and T = 150ºC.

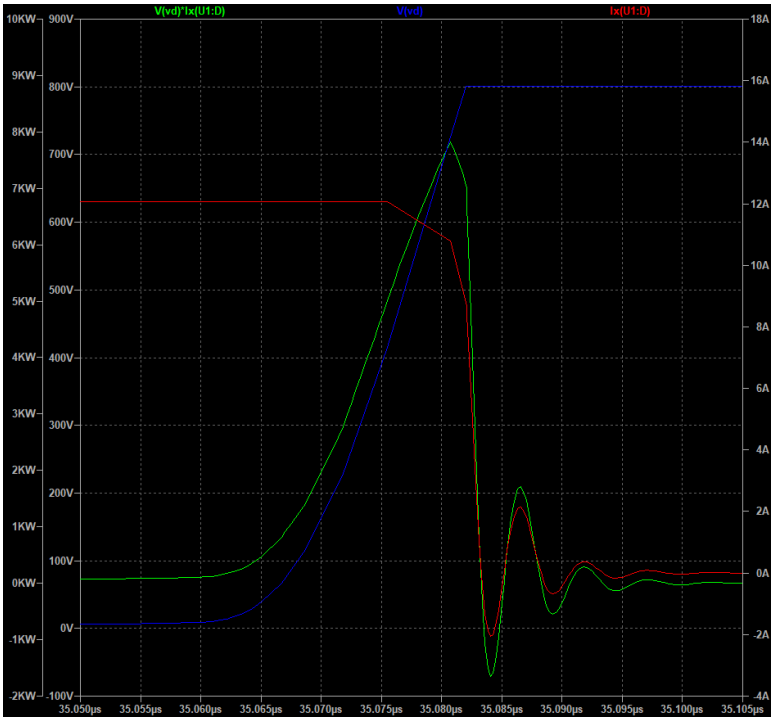

Fig. 8: Simulated turn-off transient and turn-off loss estimation for NTH4L040N120SC1 at Vds=800V, Id=12A and T = 25ºC.

Using the simulation data from the LTSPICE simulations for the IMZA65R039M1HXKSA1 and NTH4L040N120SC1 SiC MOSFETs, the switching loss parameters have been saved as look-up tables in PLECS. These look-up tables contain turn-on and turn-off switching loss data

as a function of blocking voltage and load current. The visual representation of these look-up tables for the turn-on and turn-off losses for the NTH4L040N120SC1 SiC MOSFET are shown in Figs. 9 and 10. Similarly, the switching loss data extracted from the LTSPICE simulations for the IMZA65R039M1HXKSA1 SiC MOSFET are shown in Figs. 11 and 12. For the C3M0015065K SiC MOSFET, the look-up tables containing the switching losses as a function of blocking voltage and load current, were taken from the manufacturer. The visual plotting of the turn-on and turn-off switching loss look-up tables for the C3M0015065K SiC MOSFET are presented in Figs. 13 and 14.

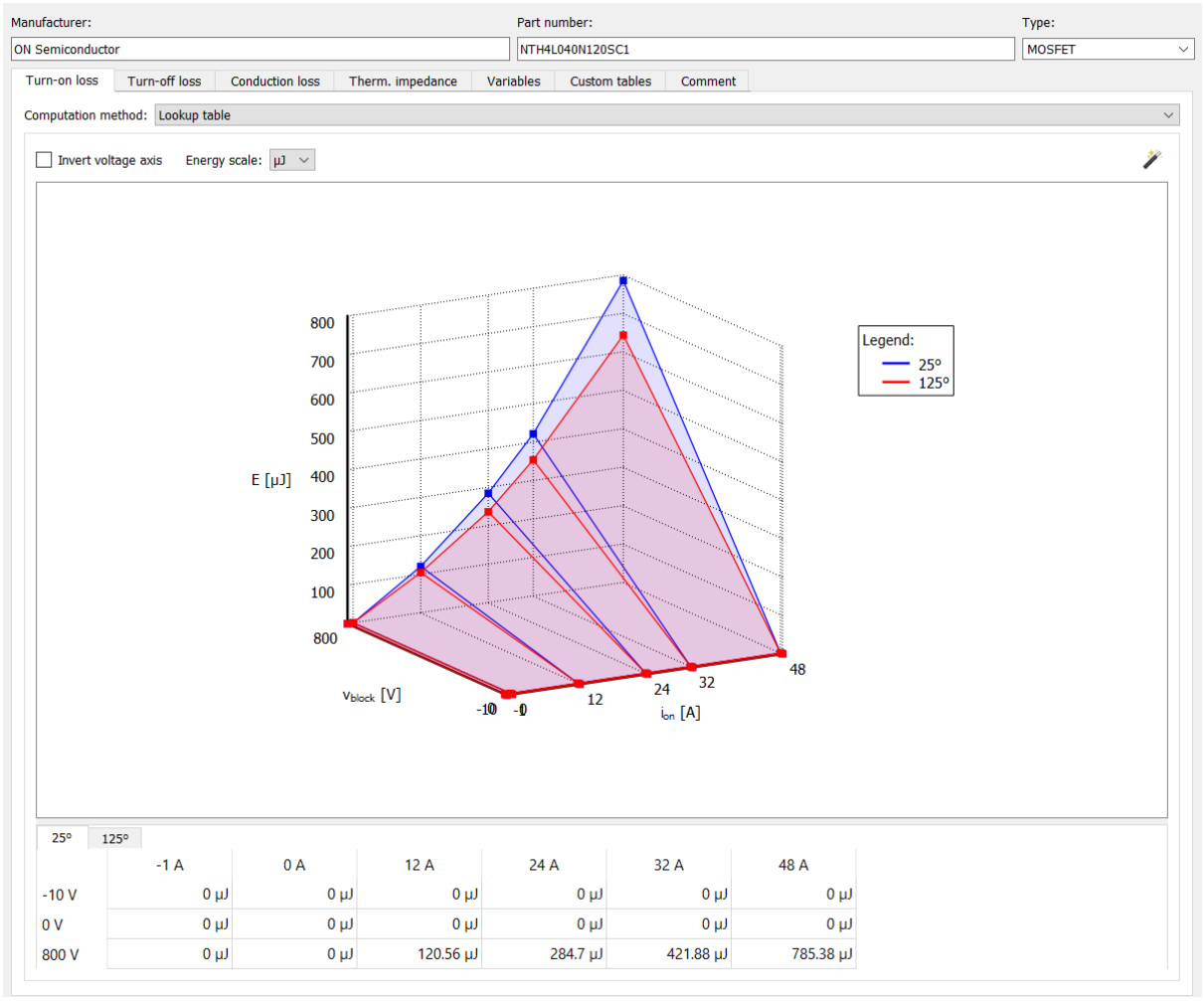

Fig. 9: Visual plotting of the PLECS look-up table with turn-on switching energies for NTH4L040N120SC1 SiC MOSFET at various blocking voltage and load current conditions.

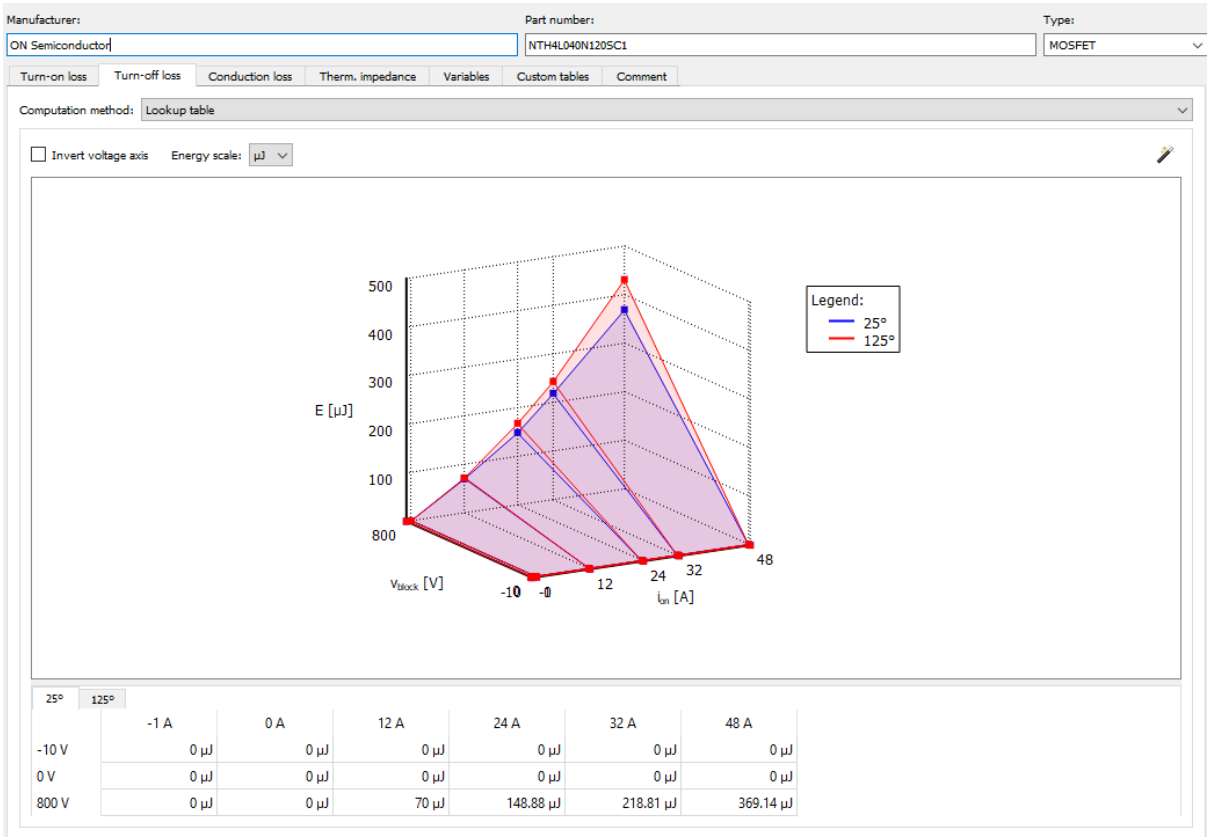

Fig. 10: Visual plotting of the PLECS look-up table with turn-off switching energies for NTH4L040N120SC1 SiC MOSFET at various blocking voltage and load current conditions.

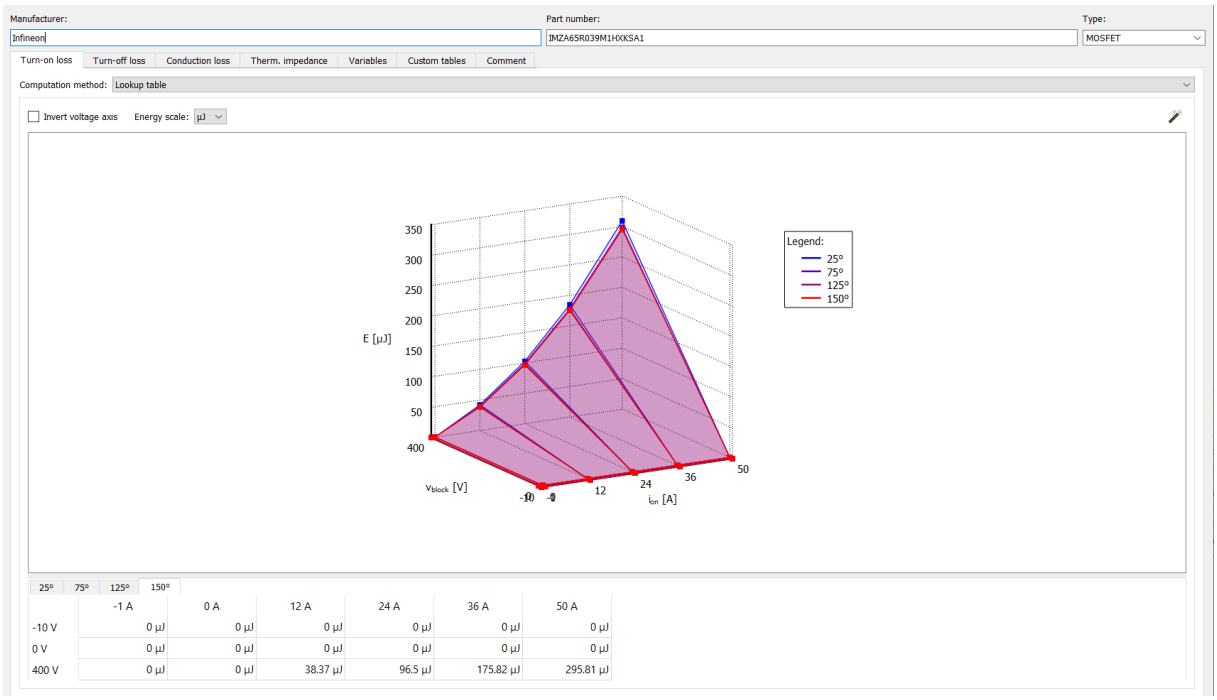

Fig. 11: Visual plotting of the PLECS look-up table with the turn-on switching energies for the IMZA65R039M1HXKSA1 SiC MOSFET.

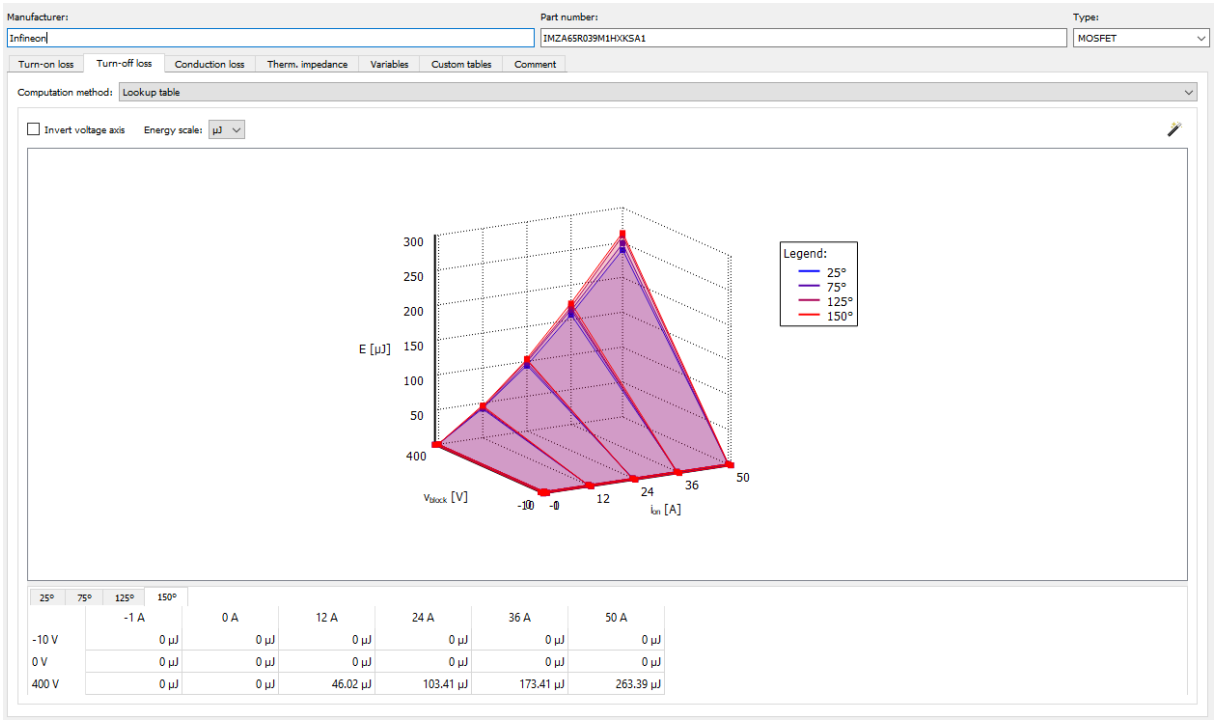

Fig. 12: Visual plotting of the PLECS look-up table with the turn-off switching energies for the IMZA65R039M1HXKSA1 SiC MOSFET.

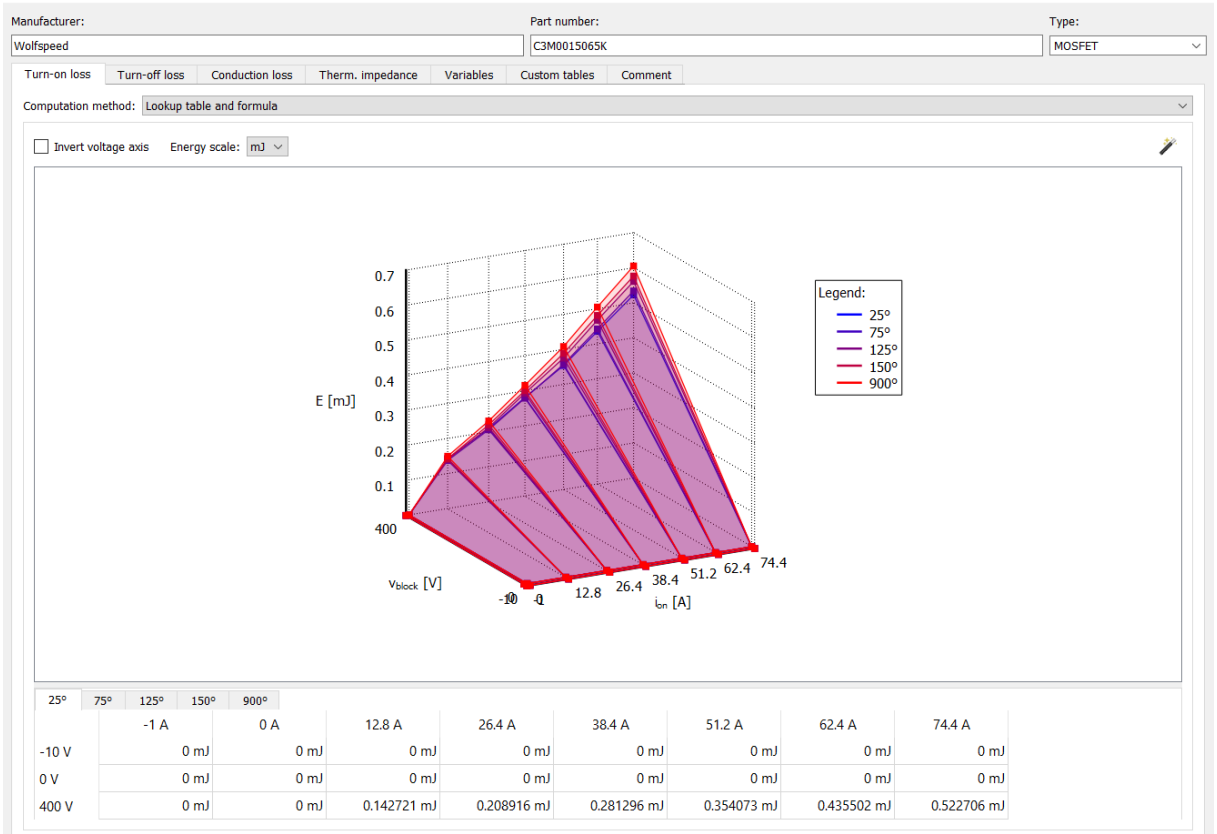

Fig. 13: Visual plotting of the PLECS look-up table with the turn-on switching energies for the C3M0015065K SiC MOSFET.

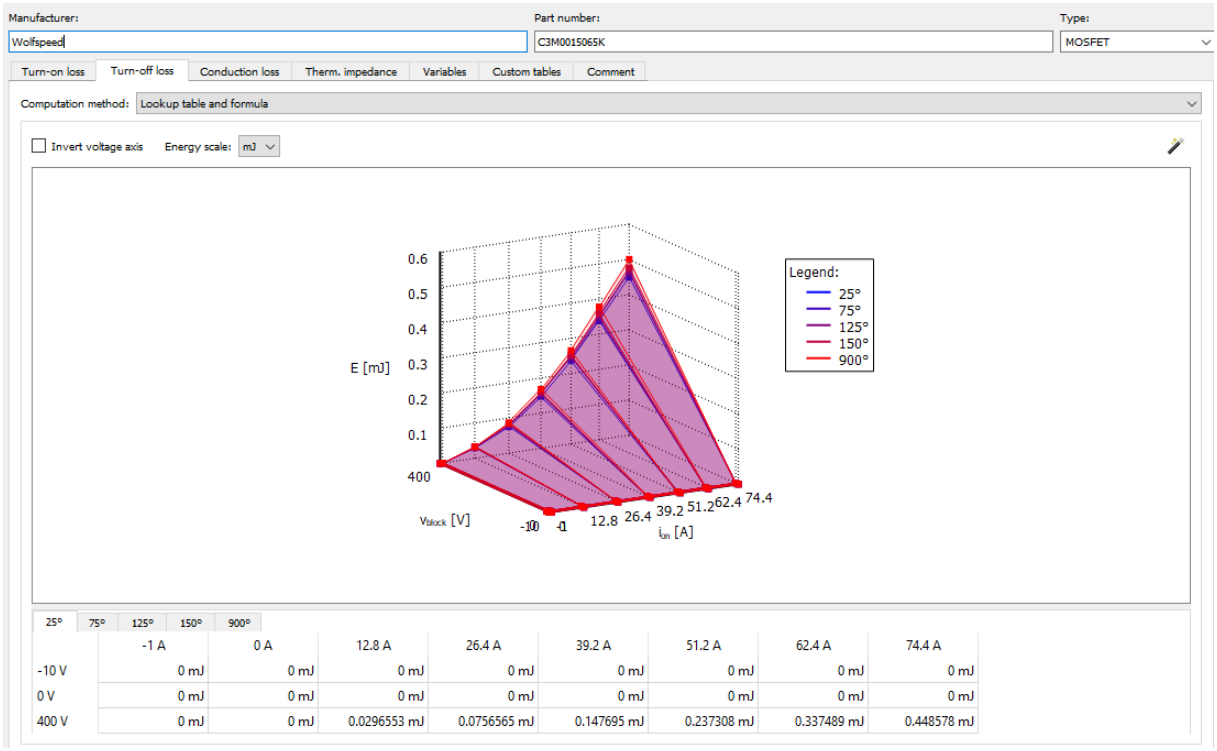

	-1 A	0 A	12.8 A	26.4 A	39.2 A	51.2 A	62.4 A	74.4 A
-10 V	0 mJ	0 mJ	0 mJ	0 mJ	0 mJ	0 mJ	0 mJ	0 mJ
0 V	0 mJ	0 mJ	0 mJ	0 mJ	0 mJ	0 mJ	0 mJ	0 mJ
400 V	0 mJ	0 mJ	0.0296553 mJ	0.0756565 mJ	0.147695 mJ	0.237308 mJ	0.337489 mJ	0.448578 mJ

Fig. 14: Visual plotting of the PLECS look-up table with the turn-off switching energies for the C3M0015065K SiC MOSFET.

The conduction loss parameters for the three types of SiC MOSFETs considered in this report, have also been modelled in look-up table format in PLECS. The on-state voltage drops of each SiC MOSFET was extracted from the datasheets as a function of load current and at various junction temperatures. The visual illustration of the look-up tables containing the conducting parameters of the three SiC MOSFETs are shown in Figs. 15-17.

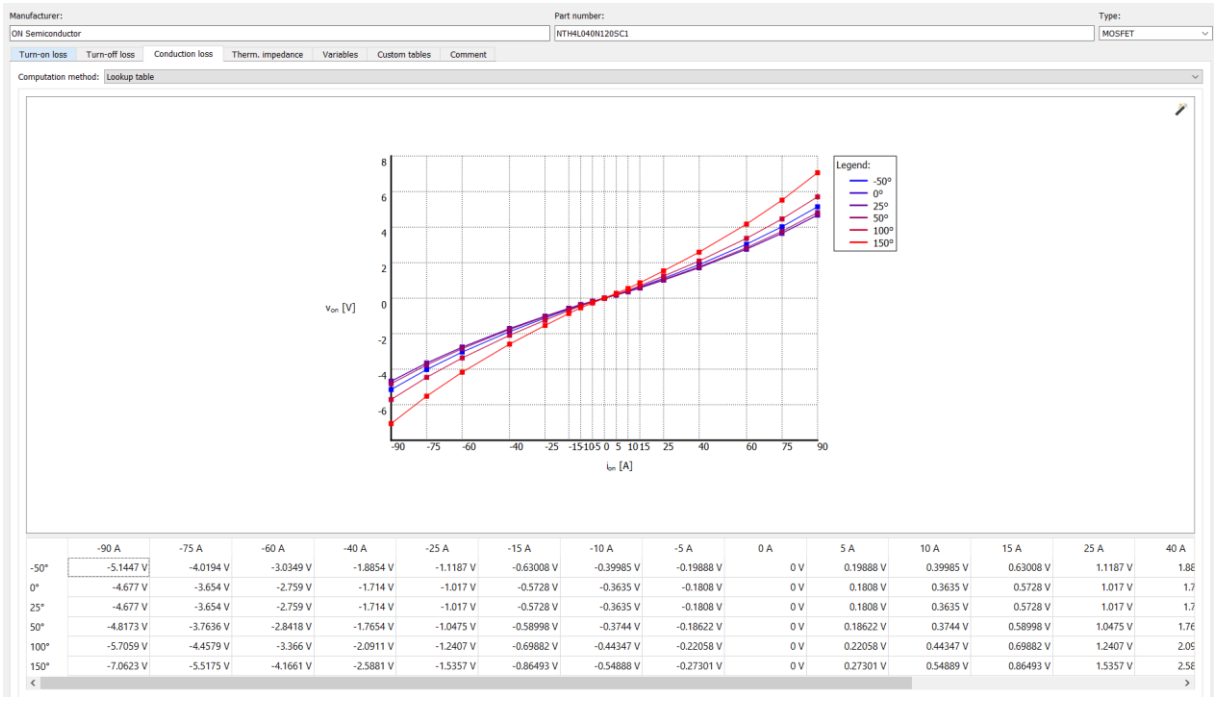

	-90 A	-75 A	-60 A	-40 A	-25 A	-15 A	-10 A	-5 A	0 A	5 A	10 A	15 A	25 A	40 A
-50°	-5.1447 V	-4.0194 V	-3.0349 V	-1.8854 V	-1.1187 V	-0.63008 V	-0.39985 V	-0.19888 V	0 V	0.19888 V	0.39985 V	0.63008 V	1.1187 V	1.86
0°	-4.677 V	-3.654 V	-2.759 V	-1.714 V	-1.017 V	-0.5728 V	-0.3635 V	-0.1808 V	0 V	0.1808 V	0.3635 V	0.5728 V	1.017 V	1.7
25°	-4.677 V	-3.654 V	-2.759 V	-1.714 V	-1.017 V	-0.5728 V	-0.3635 V	-0.1808 V	0 V	0.1808 V	0.3635 V	0.5728 V	1.017 V	1.7
50°	-4.8173 V	-3.7636 V	-2.8418 V	-1.7654 V	-1.0475 V	-0.58998 V	-0.3744 V	-0.18622 V	0 V	0.18622 V	0.3744 V	0.58998 V	1.0475 V	1.76
100°	-5.7059 V	-4.4579 V	-3.366 V	-2.0911 V	-1.2407 V	-0.69882 V	-0.44347 V	-0.22058 V	0 V	0.22058 V	0.44347 V	0.69882 V	1.2407 V	2.09
150°	-7.0623 V	-5.5175 V	-4.1661 V	-2.5881 V	-1.5357 V	-0.86493 V	-0.54888 V	-0.27301 V	0 V	0.27301 V	0.54889 V	0.86493 V	1.5357 V	2.58

Fig. 15: Visual plotting of the PLECS look-up table with conduction loss parameters for NTH4L040N120SC1 SiC MOSFET at various junction temperatures.

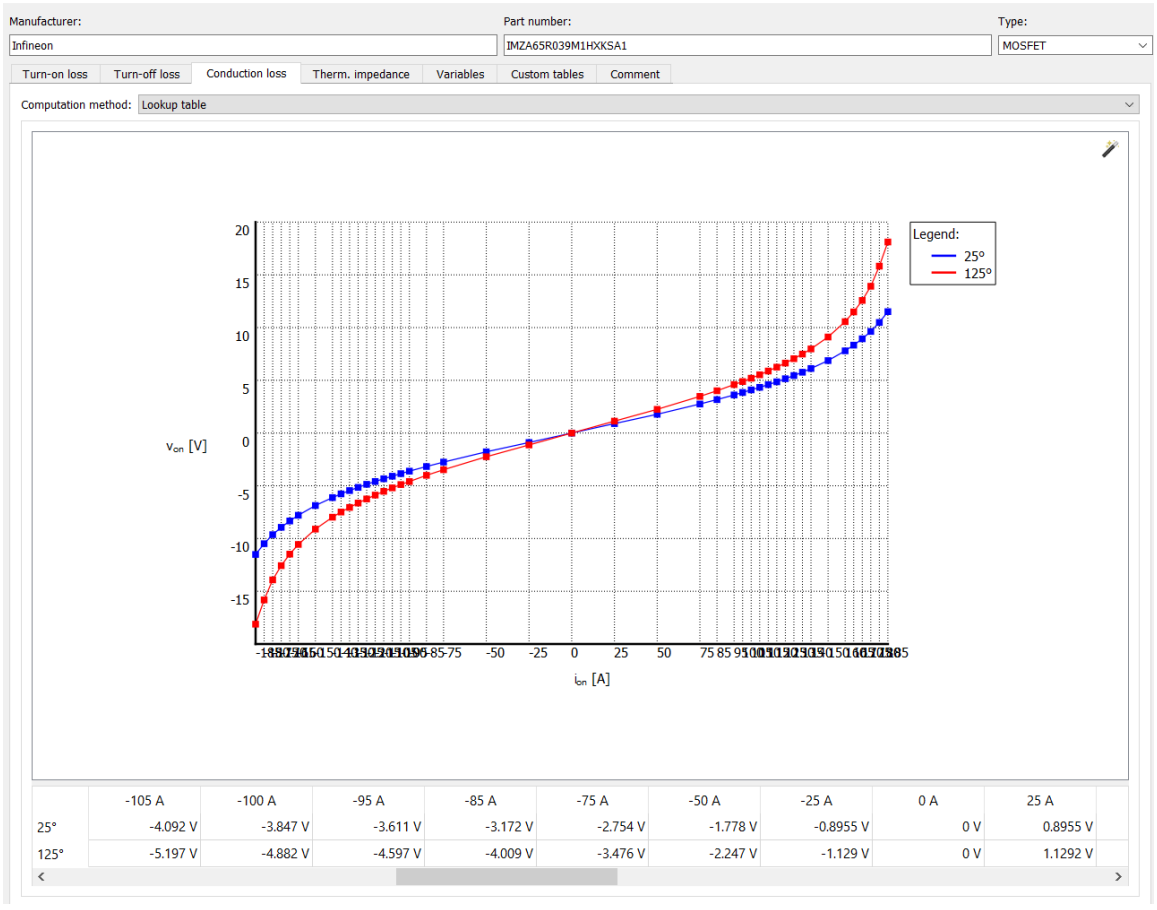

	-105 A	-100 A	-95 A	-85 A	-75 A	-50 A	-25 A	0 A	25 A
25°	-4.092 V	-3.847 V	-3.611 V	-3.172 V	-2.754 V	-1.778 V	-0.8955 V	0 V	0.8955 V
125°	-5.197 V	-4.882 V	-4.597 V	-4.009 V	-3.476 V	-2.247 V	-1.129 V	0 V	1.1292 V

Fig. 16: Visual plotting of the PLECS look-up table with conduction loss parameters for IMZA65R039M1HXKSA1 SiC MOSFET.

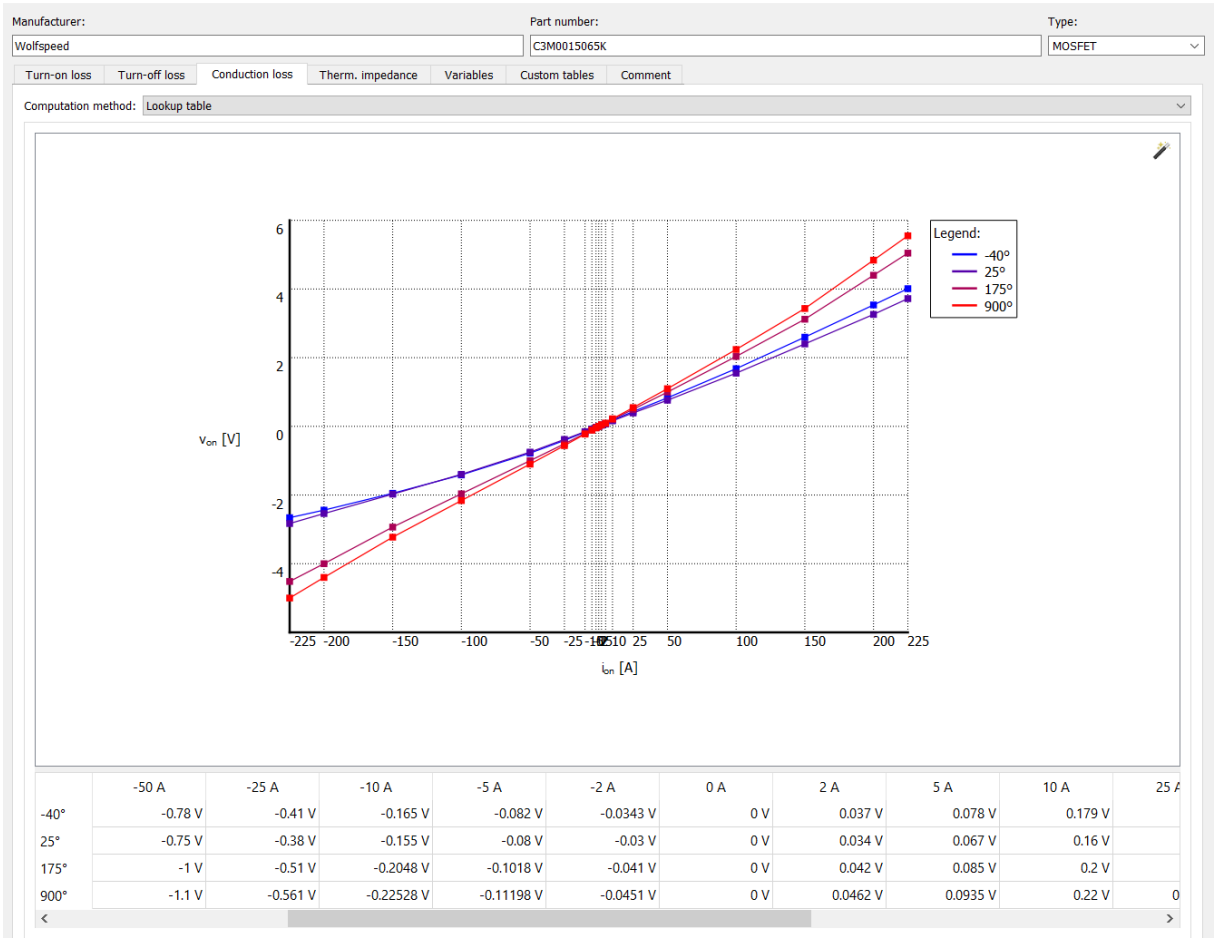

Fig. 17: Visual plotting of the PLECS look-up table with conduction loss parameters for C3M0015065K SiC MOSFET.

The high-frequency transformer of the dual active bridge is modelled using the ideal transformer component. The primary and secondary leakage inductances and the series resistances of the transformer windings are modelled as separate components. Fig. 18 shows such a model for the multi-winding transformer used in the three-port converter configurations.

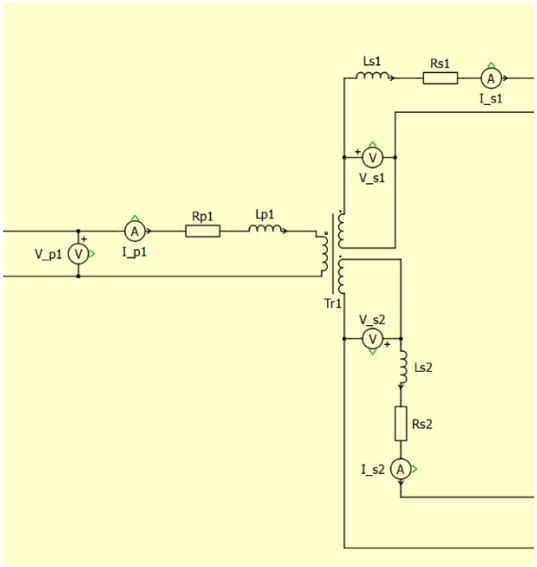

Fig. 18: Multi-winding transformer model from PLECS.

The junction temperatures of SiC MOSFETs were estimated using the PLECS thermal environment. In the thermal environment, heat sinks with custom thermal resistance and thermal capacitance can be modelled in addition to setting the value of the desired ambient temperature. An example of a heat sink PLECS model is shown in Fig. 19 (purple box).

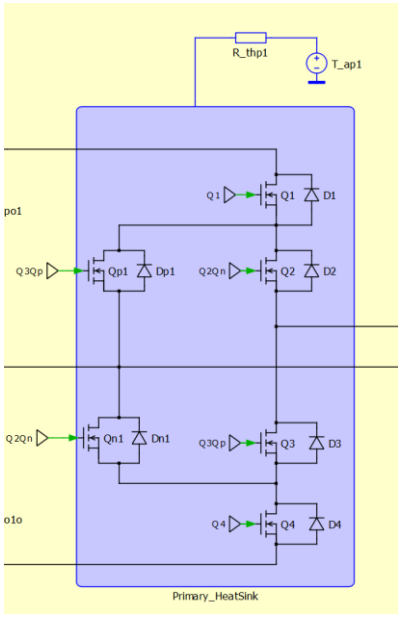

Fig. 19: PLECS simulation model of a heat sink of an ANPC bridge with a set ambient temperature, T_ap1, and thermal resistance to ambient, R_thp1.

3. Design and simulation parameters of the converters

The power transfer equation for a non-resonant DAB converter operating with single phase-shift (SPS) modulation is given by:

$$P_{out} = N * V_{primary} * V_{secondary} * \frac{\left(D * (1 - D)\right)}{2 * f_{sw} * L} \quad (1)$$

Where, D is the phase-shift ratio (0 < D < 1) between primary and secondary bridges. The value of inductor, L is calculated according to Eqn. 1 for a phase shift of D = 0.5 and for twice the nominal power level. The reason for this approach is to ensure lower reflow power at the nominal operating point, where reflow power refers to the power flow back to the source caused by circulating currents in the converter. Reflow power causes higher power losses in the bridges, thus reducing the anticipated efficiency.

The values considered for dc input voltage (V_{in}), DC output voltage (V_{out}), output power (P_{out}), switching frequency (f_{sw}), leakage inductance (L), transformer turns ratio (N) and thermal resistance of heatsink for each bridge (R_{th}) are summarized in Table II.

Table II: Design parameters of the converters

V_{in}	750V/1500V*
V_{out}	800 V
P_{out}	10 kW
f_{sw}	100 kHz
L	9µH – 70µH**
N	$V_{primary}/V_{secondary}$
R_{th}	0.175 °C/W

$V_{primary}$ - peak transformer primary voltage

$V_{secondary}$ - peak transformer secondary voltage

* Three-port FB-FB DAB and one case of three-port ANPC-FB DAB have V_{in} = 750V, all other topologies have V_{in} = 1500V

**Calculated using Eqn.1 depending on topology

The switching frequency, f_{sw} is chosen to be 100 kHz as a fair trade-off between the heat sink size, the size of magnetics and the switching losses. The thermal resistance was determined based on the datasheet of LA6/150/24V aluminium extruded heat sink from Fischer elektronik.

The choice of power semiconductor devices must be made based on the anticipated optimal performance of the specific configuration. For the investigated DC/DC isolated modular and multiport converters, SiC MOSFETs have been chosen. The specific voltage ratings should be chosen based on the DC bus voltage constraint (in this case 1.5 kV). On the other hand, the current ratings should be chosen by considering the electric power processed by each fundamental circuit, as well as the thermal effect (i.e., temperature) and the utilised cooling system under normal operation.

The chosen types of SiC power devices for achieving optimal operation of the presented modular and multiport DC/DC converter configurations are summarized in Table I. For the optimal design of the modular and multiport DC/DC converters, the optimal choice of the voltage-current ratings of the employed SiC MOSFETs must be made. Table III shows the required volt-ampere ratings for the primary and secondary bridges in each of the five presented configurations.

TABLE III: VA rating of SiC MOSFETs

Topology	Volt-Ampere rating of MOSFETs (kVA)		
FB-FB modular DAB	Primary bridge	Secondary bridge	Total
	556.8 (8 * 1200V * 58A)	624 (8 * 650V * 120A)	1180.8
ANPC-FB modular DAB	390 (12 * 650V * 50A)	624 (8 * 650V * 120A)	1014
Three-port FB-FB DAB	278.4 (4 * 1200V * 58A)	624 (8 * 650V* 120A)	902.4
Three-port ANPC-FB DAB (Vin = 750V)	195 (6 * 650V * 50A)	624 (8 * 650V* 120A)	819
Three-port ANPC-FB DAB (Vin = 1500V)	417.6 (6 * 1200V * 58A)	624 (8 * 650V* 120A)	1041.6

4. *Electrical performance – Simulation study*

The five isolated DC/DC converter configurations (2 modular and 2 multiport from which one having two input voltage options) have been modelled and simulated in PLECS, considering the parameters summarized in Table II. Fig. 20 shows the primary and secondary transformer voltages on both modules of the FB-FB modular DAB converter (Fig. 1(a)), when the input voltage to each primary bridge is 750 V and the output voltage equals 800 V. Moreover, the transformer primary and secondary currents are also plotted in this figure, when single-phase-shift modulation is applied.

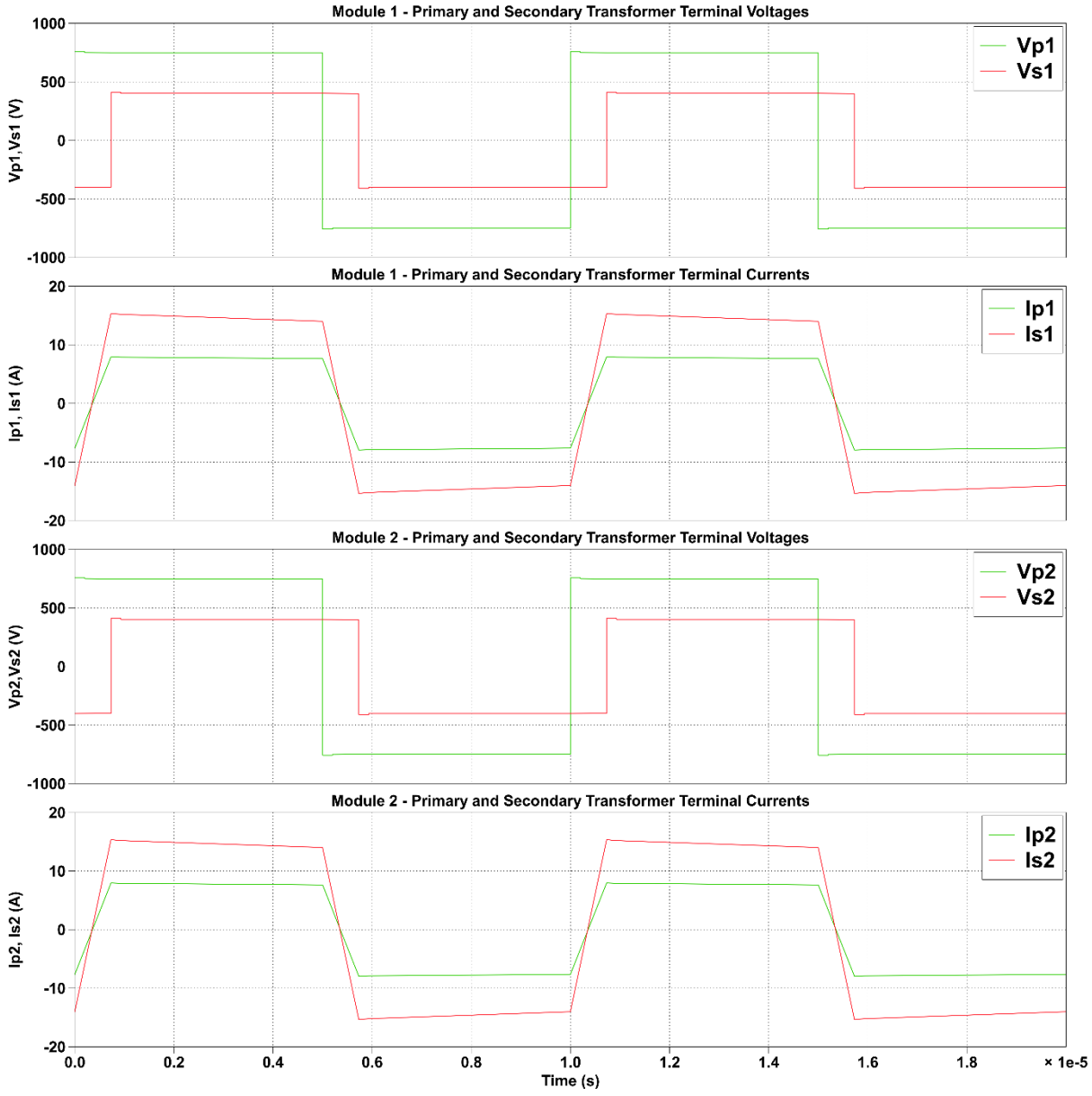

Fig. 20: (a) Transformer terminal voltages and currents for FB – FB modular DAB

Fig. 21 presents the electrical performance simulation results of the ANPC-FB modular DAB converter (Fig. 1(b)), when each primary module is fed with 750 V and the total output voltage equals 800 V. It is observed that the peak of the primary transformer voltages equal 375 V, which also dictate the use of SiC MOSFET rated at 650 V. As expected, the peak value of the output voltage is equal to 400 V, which -given the series connection of the output stages- results in a total output voltage of 800 V.

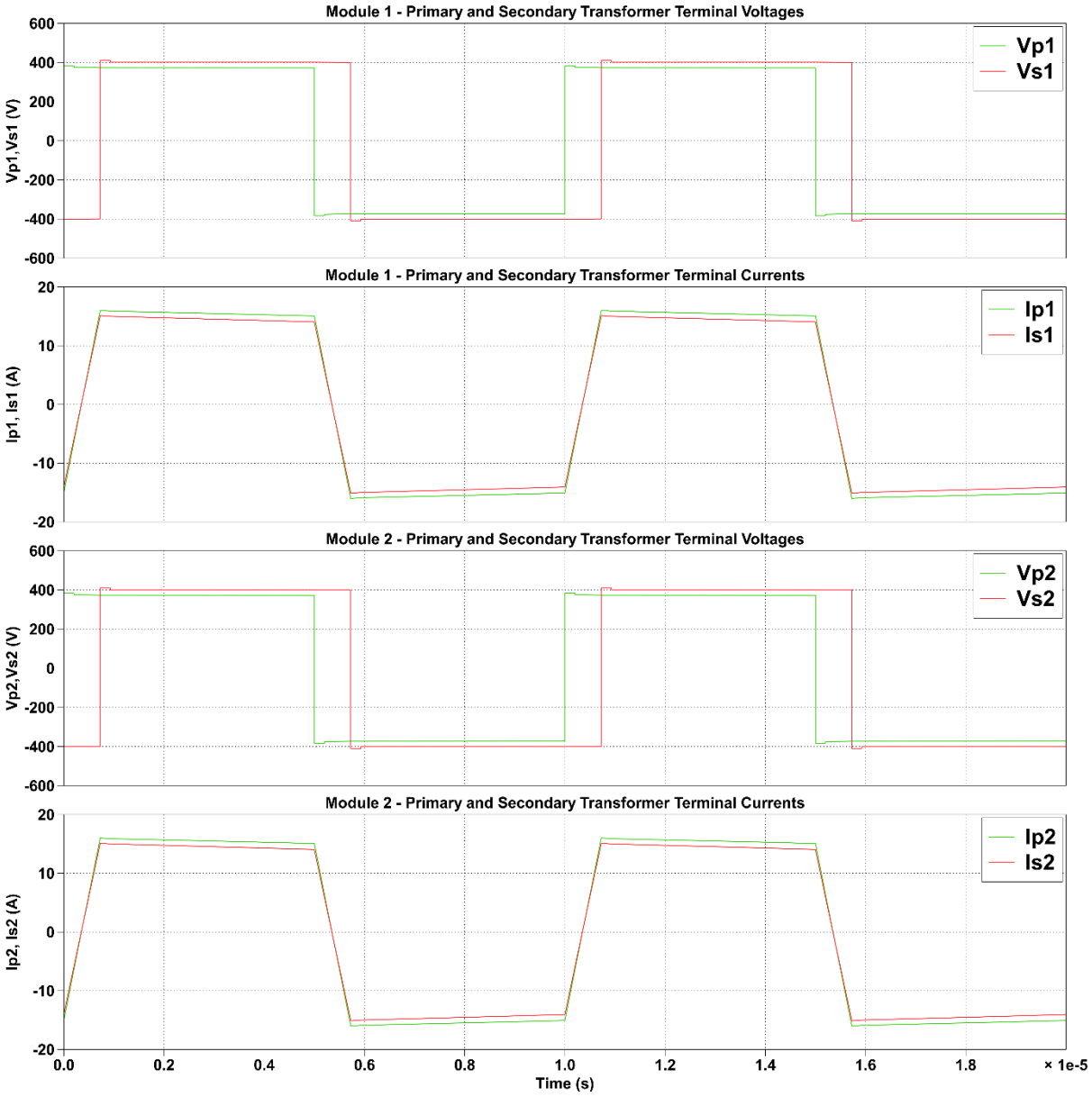

Fig. 21: (b) Transformer terminal voltages and currents for ANPC – FB modular DAB

The simulation results demonstrating the electrical performance of the three-port FB-FB configuration (Fig. 1(c)) are shown in Fig. 22. In this case, the primary bridge is supplied by 750 V and each secondary module feeds 400 V on its output; thus, the total output voltage equals 800 V. It is observed that the peak of the primary transformer voltages equal 750 V, which impose the need for employing SiC MOSFET rated at 1.2 kV. On the other hand, the secondary bridges block 400 V, thus 650-V class SiC MOSFET are sufficient. As expected, the output voltage is equal 800 V.

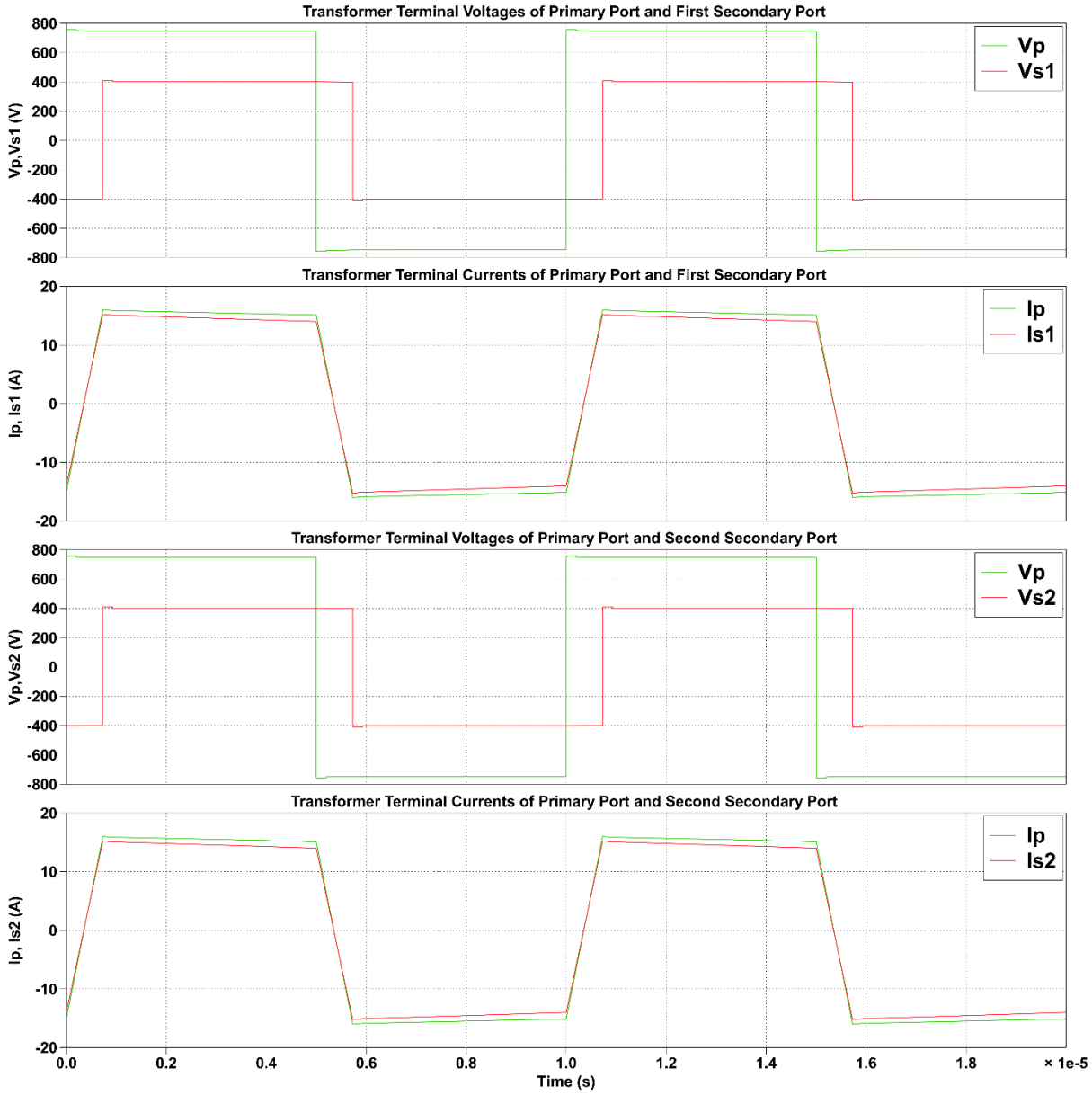

Fig. 22: (c) Transformer terminal voltages and currents for three-port FB-FB DAB

The simulation results demonstrating the electrical performance of the three-port ANPC-FB configuration (Fig. 1(d)) in the case that the primary ANPC bridge is supplied by V_{in}=750 V are shown in Fig. 23. In this case, the SiC MOSFETs employed in the primary bridge are rated at 650 V, since they have to block 375 V. The output voltage of each FB module on the secondary side equals 400 V, which impose the use of 650 V-class SiC MOSFETs. The same simulation results for the same configuration but with V_{in}=1500 V are shown in Fig. 24. In this case, the primary bridge must block 750 V, which requires 1.2-kV class SiC MOSFETs, while the design of the secondary bridges in terms of rated voltages remains the same as in the case depicted in Fig. 23. The main difference between the two cases shown in Figs. 23 and 24 is the reduced primary current stress in case that V_{in}=1.5 kV. Given that the current is governed by the voltage difference across the leakage inductance of the transformer, having a larger voltage across this, results in a higher current, and thus higher losses. The primary and secondary transformer current become almost equal in the case with V_{in}=1.5 kV (Fig. 24).

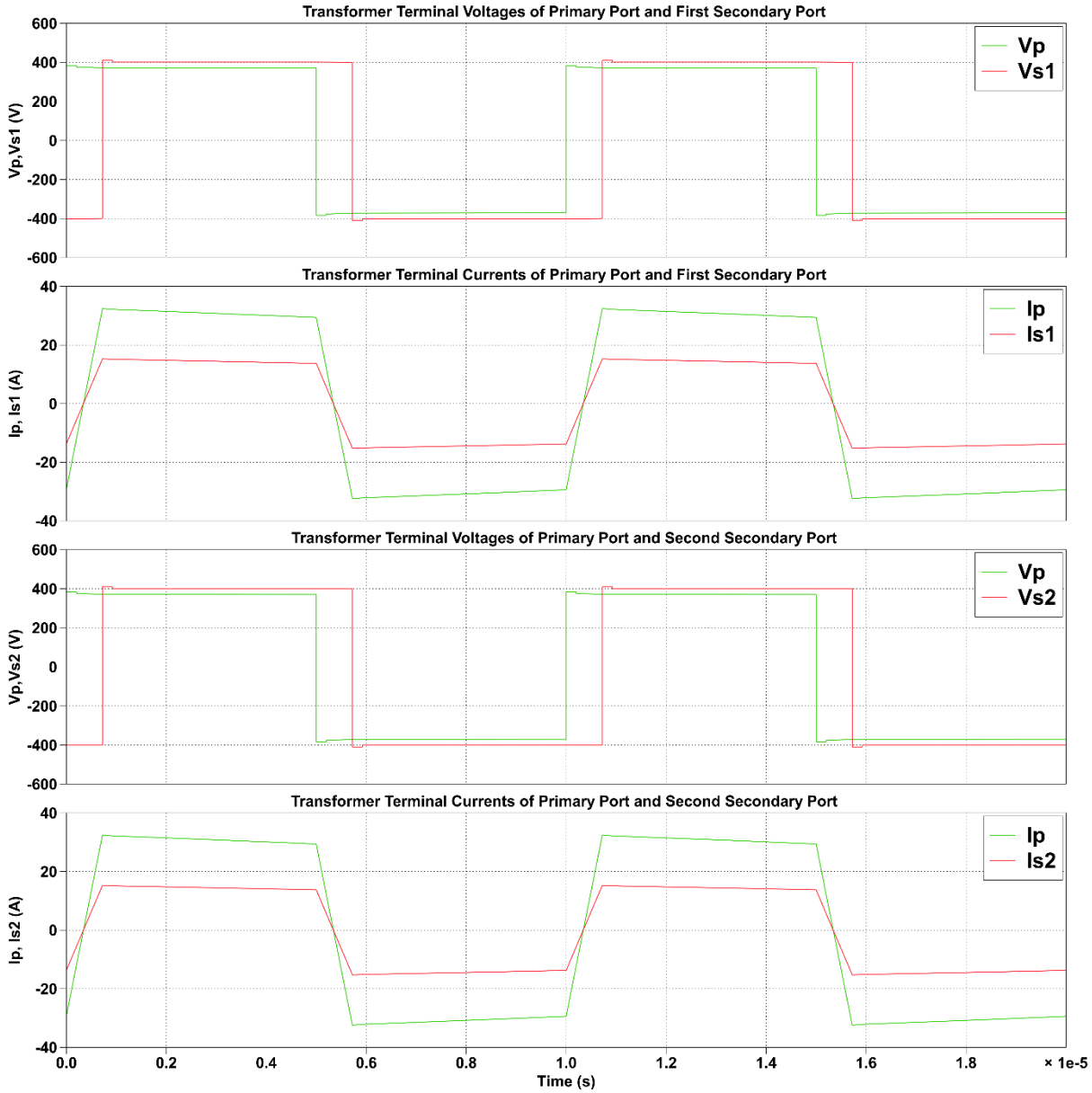

Fig. 23: (d) Transformer terminal voltages and currents for three-port ANPC-FB DAB (V_{in} = 750V)

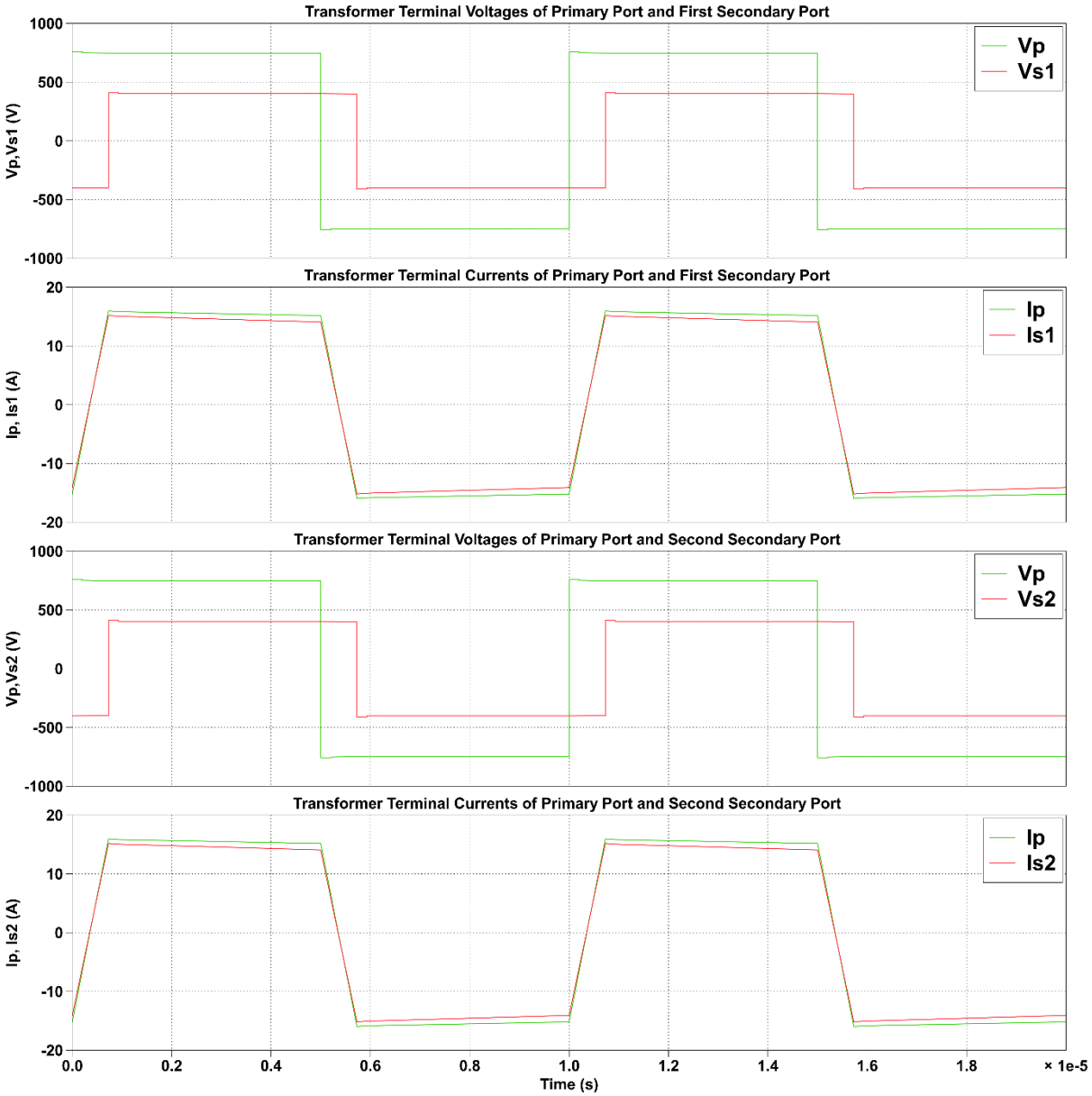

Fig. 24: (e) Transformer terminal voltages and currents for three-port ANPC-FB DAB (V_{in} = 1500V)

Using the PLECS simulation models of the five converter configurations (five due to the two input voltage options in the three-port ANPC-FB converter), the power losses and efficiencies have been extracted. The simulated efficiencies at rated conditions for the five converter configurations are shown in Fig. 25. It must be noted that these efficiency values have been extracted by considering only the switching and conduction power losses using the developed thermal models, as analysed in Section 3. From the bar plot in Fig. 25, it is observed that the lowest efficiency is achieved for the three-port ANPC-FB DAB when it is supplied by V_{in}=750 V. On the other hand, the highest efficiency is achieved for the FB-FB modular DAB, while the three-port FB-FB DAB and the three-port ANPC-FB DAB with V_{in}=1500 V exhibit the same efficiency.

The difference in efficiencies between the converter configurations is mainly dictated by the power losses in the primary bridge of each configuration as seen from Fig. 26 (i)-(v). Among the modular configurations, the primary bridge of the FB-FB modular DAB exhibits lower

conduction losses compared to the primary bridge of the ANPC-FB modular DAB. This is because, for the same transferred power, the transformer primary current of the ANPC-FB modular DAB is almost twice that of the FB-FB modular DAB. Since the two multi-port configurations (i.e., three-port FB-FB DAB and three-port ANPC-FB DAB with V_{in} = 1500V) have the same transformer primary voltage and current conditions, they exhibit the same efficiency. In case of the FB-FB modular DAB, the primary conduction loss is calculated as the sum of conduction losses in the two primary FBs, each operating at half the rated power. The transformer primary voltages at the two primary bridges are the same when compared to the primary bridge of the multi-port DAB configurations. However, the transformer primary current in each primary bridge of FB-FB modular DAB is half the transformer primary current of the multi-port DABs (see Figs. 24 (a), (c) and (e)). Therefore, the FB-FB modular DAB exhibits better efficiency compared to the multi-port DABs.

Observing, however, the power loss distribution between the primary and secondary bridges for the five configurations, it is revealed that the FB-FB modular DAB and the three-port ANPC-FB DAB with V_{in}=750 V exhibit the most uneven loss distribution, as shown in Fig. 26. This will also impact the temperatures distribution of the SiC MOSFETs and will impose different design constraints for the cooling system.

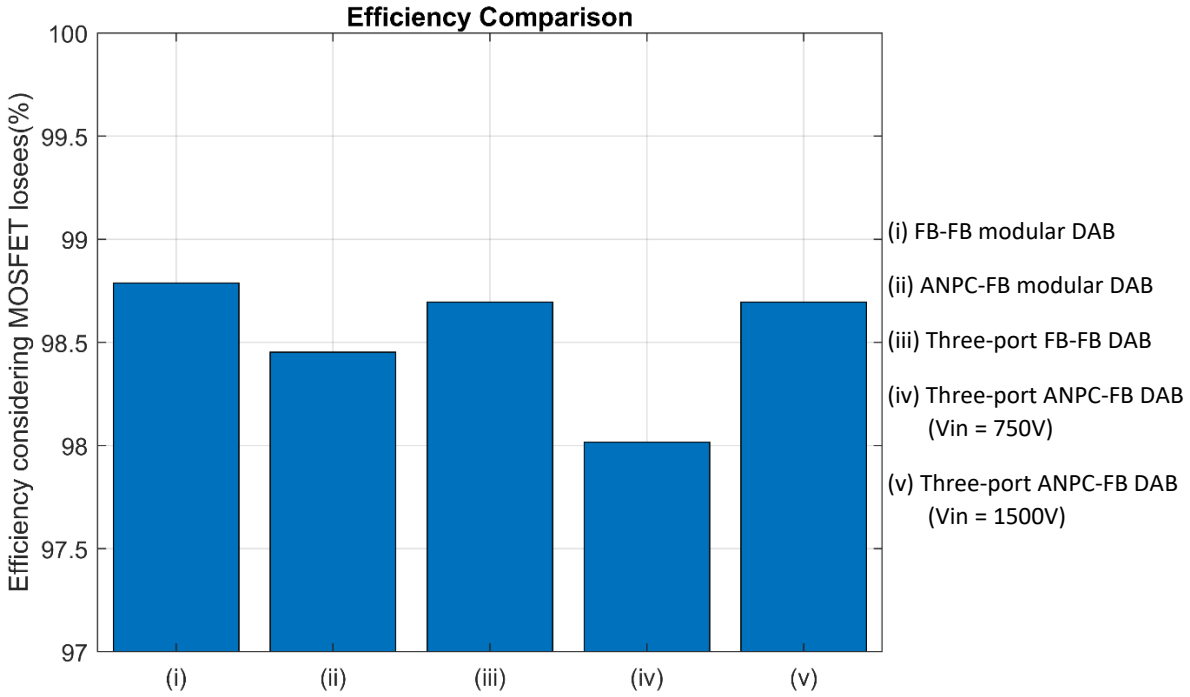

Fig. 25: Comparison of efficiency considering only the MOSFET losses based on simulations.

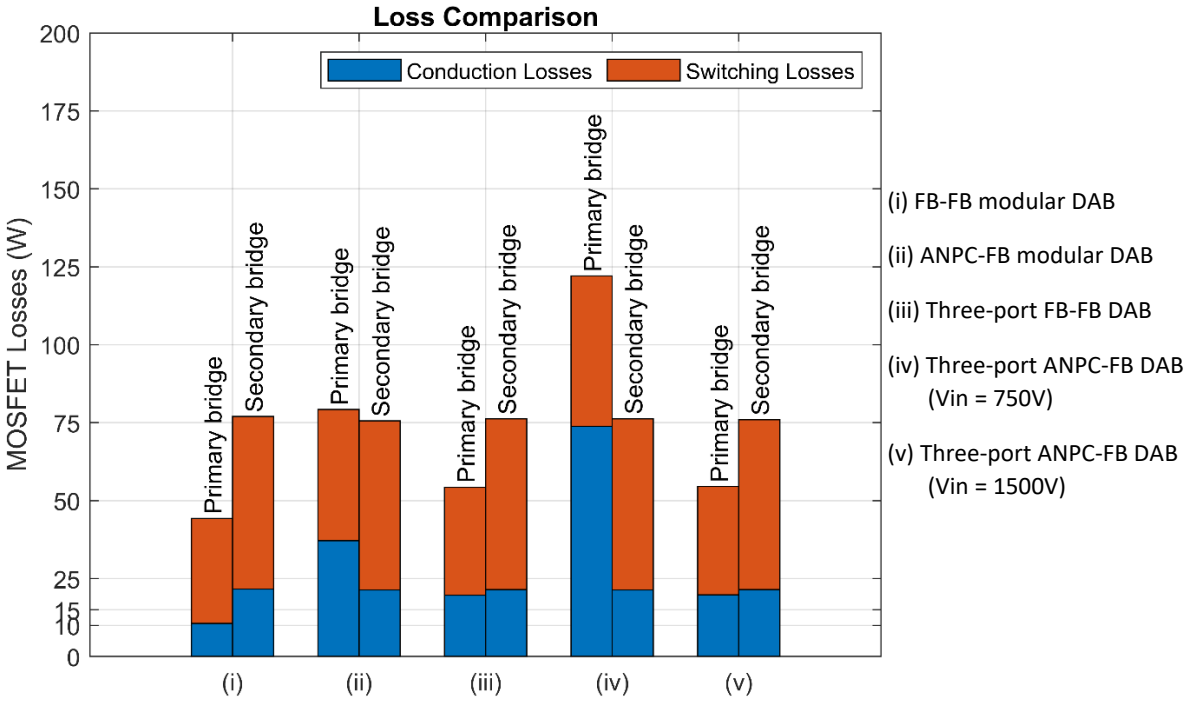

Fig. 26: Comparison of MOSFET loss distribution based on simulations.

5. *Thermal performance – Simulation study*

Fig. 27 illustrates a bar plot of the average junction temperatures for the five converter configurations based on PLECS thermal simulations.

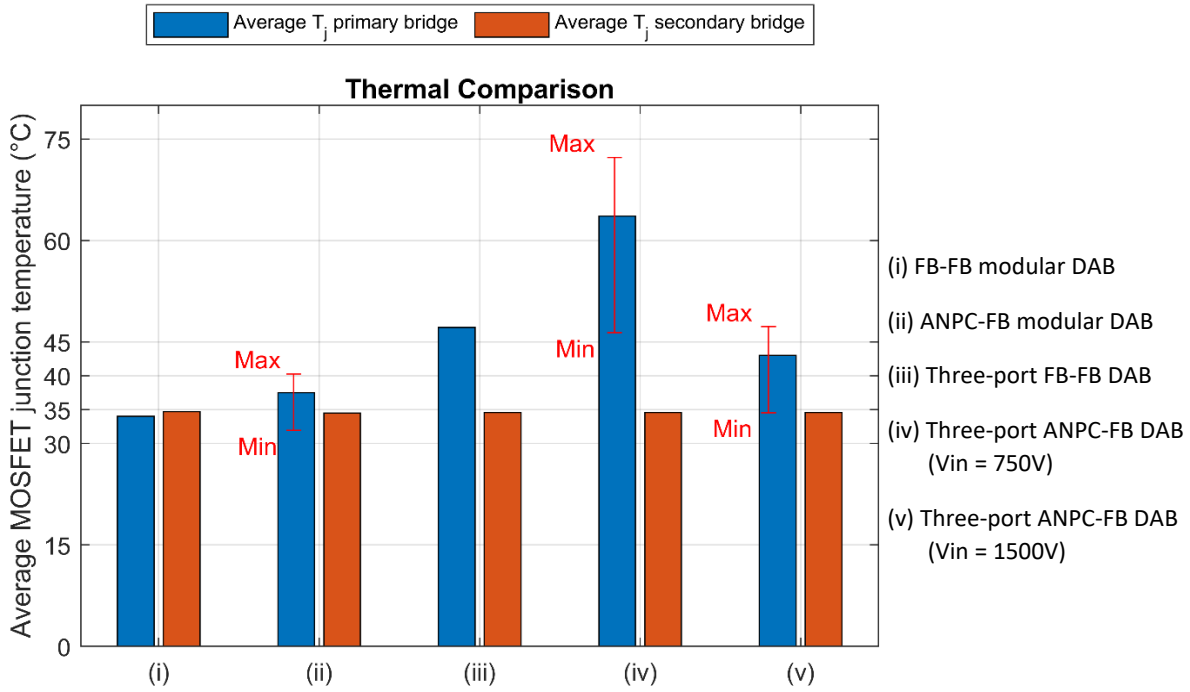

Fig. 27: Comparison of the average junction temperature in each bridge of the evaluated topologies.

In case of the FB module, all four MOSFETs have approximately the same junction temperatures due to their equal switching time periods. This is revealed by observing the orange

bars in Fig. 27. Moreover, in case of the FB-FB modular DAB ((i) in Fig. 27), the average junction temperatures between the primary and secondary bridges are approximately equal.

In case of the ANPC bridge, the two MOSFETs which clamp to the neutral point are not switched as much as the other four MOSFETs as Single Phase-Shift (SPS) modulation is employed. Therefore, the junction temperatures of the neutral-point clamping MOSFETs are lower compared to the other four MOSFETs employed in the same ANPC bridge. The maximum and minimum junction temperatures of the respective ANPC bridges are indicated in the bar plots (ii), (iv) and (v) in Fig. 27.

A general design constraint for the modular and multiport converters is the the maximum die temperature that was set at 100°C. The reason for this is the positive temperature coefficient for the on-state resistance of the SiC MOSFETs, contributing to higher conduction power losses and also the need for more sophisticated cooling system designs.

6. Conclusions

In this report the electrical and thermal modelling and simulation of two modular and three multiport isolated DC/DC converter configurations for a reconfigurable charging application have been presented. A detailed presentation of the electrical and thermal modelling of the SiC MOSFETs employed in the considered topologies is shown. Moreover, the VA ratings of the SiC MOSFETs required for each topology have been evaluated. It is revealed that the three-port ANPC-FB converter with V_{in}=750 V requires the lowest VA ratings of the SiC MOSFETs. However, this configuration exhibits the lowest efficiency and the largest spread of the junction temperatures between the primary and secondary bridges.

From the modular configurations, the best efficiency is achieved with the FB-FB DAB converter, and from the multiport configurations, both the three-port FB-FB DAB and the three-port ANPC-FB DAB with V_{in}=1500 V achieve the same highest efficiency. However, the latter exhibits a narrower temperature spread between the primary and secondary bridges. The largest temperature spread is observed for the three-port ANPC-FB DAB with V_{in}=750 V, which impose the need for different cooling system designs. This will eventually violate the constraint for standardized designs of the modules.

On the one hand, the advantages of using a multi-winding transformer (i.e., smaller volume and weight) in comparison to the use of multiple transformers should be considered for the selection of the topologies. On the other hand, criteria like reliability and fault riding ability becomes important while employing multiple units of the converters in an EV charging station.

Considering the efficiency, loss distribution, temperature distribution, VA semiconductor ratings required, and the criteria mentioned above, an EV charging station consisting multiple units of both FB-FB modular DAB and three-port FB-FB DAB configurations will be an optimal solution.